Models for compaction band propagation

J. W. RUDNICKI

Department of Civil and Environmental Engineering, Northwestern University, Evanston, IL 60208-3109, USA (e-mail: jwrudn@northwestern.edu)

Abstract: A compaction band is modelled as a thin, ellipsoidal heterogeneity with an imposed inelastic compactive strain and different elastic moduli from the surrounding matrix. Previously published results are used to determine the stress state in the band. For a wide variation of properties, stress conditions, and inelastic strain, the stress state in the band for aspect ratios observed in the field, 10^{-3}–10^{-4}, is indistinguishable from the result in the zero aspect ratio limit. In this limit, the compressive stress immediately adjacent to the band tip is roughly 10–100 times the far-field stress for parameters representative of field conditions. This value is relatively insensitive to the elastic mismatch between the band and the surrounding material, and is primarily controlled by the ratio of the far-field stress to twice the shear modulus times the inelastic compactive strain. This ratio is inferred to be about 0.02–0.05 from published field results, but may be several times larger for laboratory specimens. The ratio of tip to far-field stress increases with decrease of band shear modulus and becomes unbounded if both the shear modulus and aspect ratio go to zero. A combined anti-crack–dislocation model, in which a compactive relative displacement $2h$ is specified in the centre of the band and uniform traction elsewhere, predicts that for growth at constant energy release rate h is proportional to $\sqrt{L}$ where L is the half-length of the band. For an energy release rate of 40 kJ m^{-2}, inferred in an earlier study from field observations and comparable with compaction energies inferred from laboratory tests on circumferentially notched compression samples, the constant of proportionality is consistent with that inferred from laboratory observations and earlier field data.

In brittle rocks, shear deformation in localized zones is typically accompanied by dilation (porosity increase) or compaction (porosity decrease). In a limiting case, localized, roughly planar zones of solely compaction, without shear, can occur perpendicular to the maximum compressive stress. Such structures, called compaction bands, have been identified in porous sandstone formations in the field (Mollema & Antonellini 1996; Sternlof *et al.* 2005; Sternlof 2006), in axisymmetric compression experiments on several porous sandstones (Olsson 1999; Olsson & Holcomb 2000; Wong *et al.* 2001; Holcomb & Olsson 2003; Baud *et al.* 2004; Fôrtin *et al.* 2006) and emanating from borehole breakouts in laboratory experiments on porous sandstone (Haimson & Song 1998; Haimson 2001, 2003; Klaetsch & Haimson 2002; Haimson & Lee 2004). Although this mode of localized deformation has attracted attention in rocks only recently, it has been observed in a variety of other porous materials, including metal foams (Bastawros *et al.* 2000; Park & Nutt 2001), polycarbonate honeycomb (Papka & Kyriakides 1998), snow (J. Desrues, pers. comm.), ice (Kirby *et al.* 1992) and large deformation of porous elastomers (Kinney *et al.* 2001). Both laboratory (Holcomb & Olsson 2003; Vajdova *et al.* 2004) and field studies (Antonellini & Aydin 1994, 1995; Sternlof *et al.* 2004; Sternlof 2006) have shown that compaction bands can inhibit flow across them. The porous rocks in which these bands have been observed are typical of reservoir rocks. The presence of compaction bands in such formations can form impermeable barriers and adversely affect the use of these rocks for a variety of applications, such as aquifer management, hydrocarbon recovery and storage, and CO_2 sequestration (Wawersik *et al.* 2001).

There are many differences between the structures observed in the laboratory and in the field but an obvious one is their length. The lengths of bands observed in the field (Mollema & Antonellini 1996; Sternlof *et al.* 2005; Sternlof 2006) are of the order of tens of metres. In contrast, the lengths of the bands in the experiments are limited to the width of the specimen, a few centimetres. In addition, the bands in the experiments appear suddenly across the entire width, or, at least, extend across the width rapidly in comparison with the rate of loading (Wong *et al.* 2001; Baud *et al.* 2004; Fôrtin *et al.* 2006). The constraint created by the larger amount of material surrounding the bands in the field is certainly one factor in the differences in extension. In an effort to understand better the conditions for extension of compaction bands, Vajdova & Wong (2003) and Tembe *et al.* (2006) conducted axisymmetric compression tests on circumferentially notched specimens. They observed incremental propagation of compaction bands from the notch edge that coincided with bursts of acoustic emission activity.

From: DAVID, C. & LE RAVALEC-DUPIN, M. (eds) *Rock Physics and Geomechanics in the Study of Reservoirs and Repositories*. Geological Society, London, Special Publications, **284**, 107–125.
DOI: 10.1144/SP284.8 0305-8719/07/$15.00

One possible mechanism for band extension is that the presence of the band increases the compressive stress ahead of the band (the component perpendicular to the plane of the band or, possibly, the hydrostatic stress) to a level that favours band extension. A second, more complex possibility is that the presence of the compaction band alters the stress and deformation field just ahead of the band in a way that makes it more favourable for localized compaction according to the criterion that has been used with some success to model the onset of band formation (Issen & Rudnicki 2000; Rudnicki 2003, 2004; Bésuelle & Rudnicki 2004; Challa & Issen 2004; Grueschow & Rudnicki 2005). Essential to evaluation of either mechanism is knowledge of the stress state ahead of the band. Here we calculate the stress within the band and adjacent to the band tip using a model of the band as a flat, ellipsoidal inclusion subjected to an inelastic compactive strain and having different elastic moduli from the surrounding matrix material.

Although knowledge of the stress state ahead of the band tip is necessary to evaluate propagation, it is not sufficient. Extension of the band by localization depends on the inelastic properties of the material. For extension by elevation of the stress ahead of the band, the level of the stress needed must be known. Furthermore, the stress field at the tip of the band depends on the detailed structure there. In a later section, we summarize an energy release criterion for propagation suggested by Rudnicki & Sternlof (2005) that does not depend on the details of the near-tip field.

Finally, we examine a combined anti-crack–dislocation model motivated by a suggestion by Sternlof (2006) and by the observed variation of midpoint band width with length reported by Sternlof *et al.* (2005). The model has a closing mode dislocation, representing inelastic compaction specified over the central portion of the band and uniform traction, equal to the difference between far-field compressive normal stress and a resistive band stress, specified over the remainder. The magnitude of this traction is specified by the requirement that the relative displacement should vary smoothly at the ends of the central dislocation.

Compaction band as ellipsoidal inhomogeneity

At present, the only detailed study of compaction bands in the field is that of Sternlof (2006) on the Aztec Sandstone of the Valley of Fire, Nevada. A striking feature of these data is that profiles of the width of the bands v. length are very nearly elliptical, although the aspect ratio is very small, 10^{-3}–10^{-4}. Sternlof *et al.* (2005) figure 4a shows 1700 measurements of thickness v. length for 16 band traces. The measurements have a correlation index of 0.79 with an ellipse drawn through the data. Sternlof *et al.* figure 4c shows data for a single band 24.75 m long with a correlation index of 0.87. These data strongly suggest modelling the bands as ellipsoidal inhomogeneities, which makes it possible to take advantage of the well-known results of Eshelby (1957).

The compaction band is idealized as an ellipsoidal region with different elastic properties from the surrounding material (Fig. 1). The surrounding material is assumed to be of infinite extent (that is, of extent much greater than that of the compaction band) and loaded at infinity by compressive normal stresses in directions coinciding with the principal axes of the ellipsoid. Eshelby (1957) showed that the stress and strain in the ellipsoidal region are uniform (as long as the properties of the region are uniform). Because of the uniform interior strain and the ellipsoidal shape, the displacements of the boundary are also ellipsoidal. This supports the use of the measured width of the bands as a surrogate for the displacements in the observations of Sternlof *et al.* (2005) and Sternlof (2006).

A further implication of Eshelby's (1957) result is that the difference between the stress state in the band σ_{ij}^{B} and the stress state in the far field σ_{ij}^{∞} is related to the corresponding difference in strain states $\varepsilon_{ij}^{B} - \varepsilon_{ij}^{\infty}$ by

$$S_{mnkl}C_{klij}\left\{\sigma_{ij}^{B} - \sigma_{ij}^{\infty}\right\} = (S_{mnkl} - \delta_{mk}\delta_{nl}) \times \left\{\varepsilon_{kl}^{B} - \varepsilon_{kl}^{\infty}\right\} \qquad (1)$$

where δ_{ij} is the Kronecker delta ($\delta_{ij} = 1$, if $i = j$; $\delta_{ij} = 0$, if $i \neq j$). Here and throughout the paper, repeated indices imply summation over values 1, 2, and 3. In equation (1) the S_{mnkl} are components of a tensor that depends only on the geometry of the ellipsoid and the Poisson's ratio ν of the matrix. The tensor possesses the symmetries $S_{mnkl} = S_{nmkl}$ and $S_{mnkl} = S_{mnlk}$ but, in general, $S_{mnkl} \neq S_{klmn}$. The C_{klij} are the elastic compliances of the matrix, i.e.

$$\varepsilon_{ij}^{\infty} = C_{ijkl}\sigma_{kl}^{\infty}. \qquad (2)$$

(The result (1) was not cited explicitly by Eshelby (1957) but follows from the results of that study and has been discussed by Rudnicki (1977, 2002).) The band material is also assumed to be elastic, possibly with different properties from the matrix, but subjected to an inelastic strain ε_{ij}^{p}. Thus, the relation between the stress and strain in the band is given by

$$\varepsilon_{ij}^{B} = C_{ijkl}^{B}\sigma_{kl}^{B} + \varepsilon_{ij}^{p} \qquad (3)$$

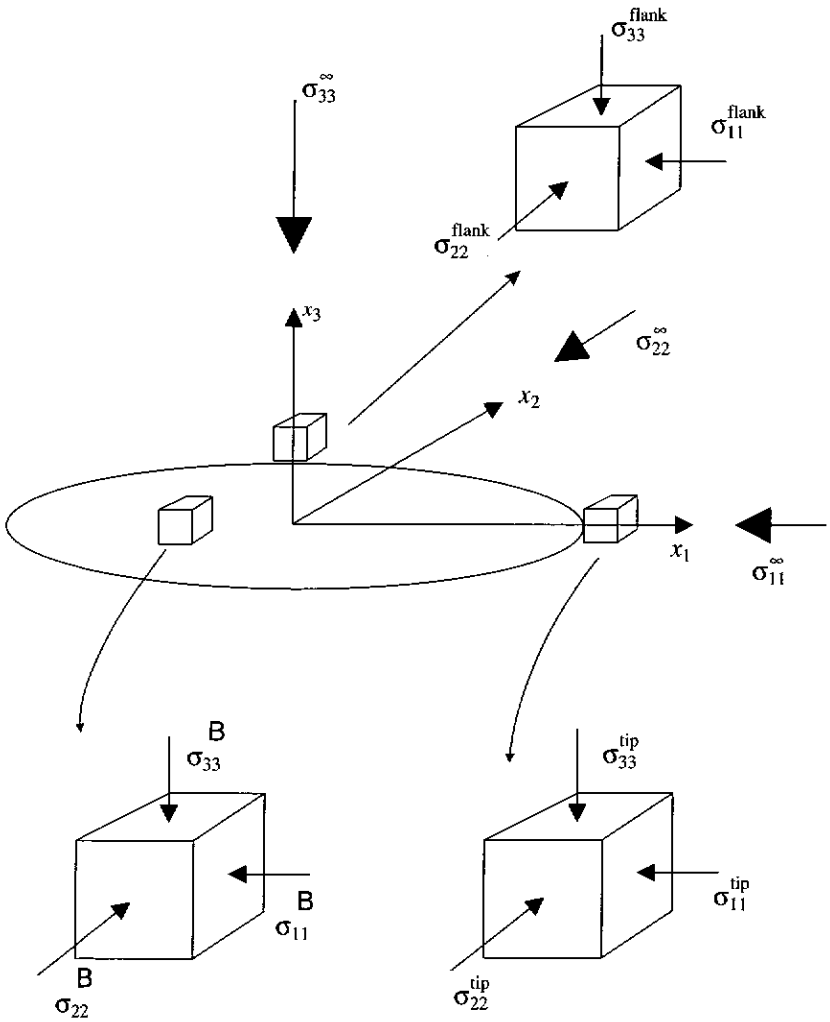

Fig. 1. Model of a compaction band as a thin, axisymmetric ellipsoidal inclusion showing far-field stresses σ_{ij}^{∞}, uniform stresses in the band σ_{ij}^{B}, stresses at the tip of the band σ_{ij}^{tip} and stresses at the flank σ_{ij}^{flank}.

where the C_{ijkl}^{B} are the elastic compliances of the band. The elasticities of both the band and the matrix are assumed to be isotropic so that the C_{ijkl} have the form

$$C_{ijkl} = \frac{1}{2\mu}\left\{\frac{1}{2}\left(\delta_{ik}\delta_{jl} + \delta_{il}\delta_{jk}\right) - \frac{\nu}{1+\nu}\delta_{ij}\delta_{kl}\right\} \quad (4)$$

where μ is the shear modulus and ν is Poisson's ratio. The corresponding array of moduli is

$$L_{ijkl} = (\kappa - 2\mu/3)\delta_{ij}\delta_{kl} + \mu\left(\delta_{ik}\delta_{jl} + \delta_{il}\delta_{jk}\right) \quad (5)$$

where $\kappa = 2\mu(1+\nu)/3(1-2\nu)$ is the bulk modulus and

$$L_{ijkl}C_{klmn} = C_{ijkl}L_{klmn} = \frac{1}{2}\left(\delta_{im}\delta_{jn} + \delta_{in}\delta_{jm}\right). \quad (6)$$

Equations (2) and (3) can be used to eliminate the stress or the strain from (1). Doing the latter gives

$$\sigma_{pq}^{B} + L_{pqmn}^{B}S_{mnkl}\left\{C_{klij} - C_{klij}^{B}\right\}\sigma_{ij}^{B} = L_{pqmn}^{B}\left\{C_{mnij}\sigma_{ij}^{\infty} - \left(\varepsilon_{mn}^{p} - S_{mnkl}\varepsilon_{kl}^{p}\right)\right\}. \quad (7)$$

If $\varepsilon_{ij}^{p} = -\zeta^{I} p^{I} C_{ijkk}^{I}$, then equation (7) reduces to equation (13) of Rudnicki (2002), where p is pore pressure in the inhomogeneity and ζ^{I} is a porous media constant; Rudnicki (2002) used the superscript I for B, G and K for the moduli denoted here by μ and κ, respectively, and labelled matrix elasticity tensors with the superscript ∞. In addition, the matrix C_{mnpq} in the first term on the right-hand side of equation (13) of Rudnicki (2002) should have the superscript I replaced by ∞. Specializing to isotropic materials, separating the stress and inelastic strain into deviatoric and spherical parts, i.e.

$$\sigma_{ij} = s_{ij} + \sigma\delta_{ij} \tag{8a}$$

$$\varepsilon_{ij}^{p} = e_{ij}^{p} + \frac{1}{3}\varepsilon^{p}\delta_{ij} \tag{8b}$$

and substituting into (7) gives the following two equations:

$$\sigma^{B}(1+\alpha k) = (k+1)\sigma^{\infty} - \kappa_{B}(1-\alpha)\varepsilon^{p} + \kappa_{B} S_{mmkl}\left(e_{kl}^{p} - g s_{kl}^{B}/2\mu_{B}\right) \tag{9}$$

and

$$s_{pq}^{B} + \left(g s_{kl}^{B} - 2\mu_{B} e_{kl}^{p}\right) \times \left\{S'_{pqkl} - \frac{k}{3(1+\alpha k)} S'_{pqkk} S_{mmkl}\right\} = (1+g)s_{pq}^{\infty} - 2\mu_{B} e_{pq}^{p} + \frac{2\mu_{B}}{3\kappa_{B}} \frac{S'_{pqkk}}{(1+\alpha k)} \times \left(\kappa_{B}\varepsilon^{p} - k\sigma^{\infty}\right) \tag{10}$$

where

$$S'_{pqkl} = S_{pqkl} - \frac{1}{3}\delta_{pq} S_{mmkl} \tag{11}$$

$g = \mu_{B}/\mu - 1$, $k = \kappa_{B}/\kappa - 1$, and

$$S_{mmkk} = 3\alpha = (1+\nu)/(1-\nu). \tag{12}$$

If $\varepsilon_{ij}^{p} = -\zeta^{I} p^{I} K_{I} \delta_{ij}$, then (9) and (10) reduce to equations (15) of Rudnicki (2002) with the changes in notation noted following (7).

Stress state in an axisymmetric band

Although it is possible to carry out the analysis for an arbitrarily shaped ellipsoid, the planform of compaction bands is not well constrained by observation and the analysis simplifies considerably if the ellipsoid is axisymmetric. Hence, the lengths of the semi-axes of the ellipsoid in the x_1 and x_2 directions are assumed to be equal to a and greater than the length c of the distinguished short axis in the x_3 direction (Fig. 1). If, in addition, the far-field stress state is axisymmetric with principal directions aligned with the band axes, and only $\sigma_{22}^{\infty} = \sigma_{11}^{\infty}$ and σ_{33}^{∞} are nonzero, then the stress state in the band is also axisymmetric, and only $\sigma_{22}^{B} = \sigma_{11}^{B}$ and σ_{33}^{B} are nonzero. In this case, for both the band and the far-field, the mean stress is related to the components by $\sigma = (2\sigma_{11} + \sigma_{33})/3$ and there is only a single distinguished deviatoric component,

$$s_{33} = -2s_{22} = -2s_{11} = 2(\sigma_{33} - \sigma_{11})/3. \tag{13}$$

Similarly, we assume that the inelastic strain is also axisymmetric so that there is only one distinguished deviatoric component

$$e_{33}^{p} = -2e_{22}^{p} = -2e_{11}^{p} = 2\left(\varepsilon_{33}^{p} - \varepsilon_{11}^{p}\right)/3. \tag{14}$$

Setting $p = q = 3$ in (10) yields

$$s_{33}^{B} = \frac{1}{1+gA}\left\{(1+g)s_{33}^{\infty} + 2\mu_{B} e_{33}^{p}(A-1) + (2\mu_{B}/\kappa_{\infty})B(\kappa_{B}\varepsilon^{p} - k\sigma^{\infty})\right\} \tag{15}$$

where

$$A = S_{3333} - S_{3311} - \frac{(1+kS_{33kk})(S_{mm33} - \alpha)}{2(1+\alpha k)} \tag{16}$$

and

$$B = \frac{(S_{33kk} - \alpha)}{3(1+\alpha k)} \tag{17}$$

and, for axisymmetry the indices '1' and '2' may be interchanged on the S_{ijkl}. Expressions for the relevant S_{ijkl} have been given by Mura (1987) and Rudnicki (2002) and, for convenience, are also listed in the Appendix. Evaluating (9) for axisymmetry then gives

$$\sigma^{B}(1+\alpha k) = (k+1)\sigma^{\infty} - \kappa_{B}(1-\alpha)\varepsilon^{p} + \kappa_{B} 2S_{mm11}\left(e_{11}^{p} - g s_{11}^{B}/2\mu_{B}\right) + \kappa_{B} S_{mm33}\left(e_{33}^{p} - g s_{33}^{B}/2\mu_{B}\right) \tag{18}$$

where $S_{mm11} = S_{mm22}$. Using (13) and (14) gives

$$\sigma^{B}(1+\alpha k) = (k+1)\sigma^{\infty} - \kappa_{B}(1-\alpha)\varepsilon^{P} + \kappa_{B}(S_{mm33} - S_{mm11}) \times \left(e^{P}_{33} - g s^{B}_{33}/2\mu_{B}\right). \quad (19)$$

However,

$$S_{mm11} = \frac{1}{2}(S_{mmkk} - S_{mm33})$$

and therefore

$$S_{mm33} - S_{mm11} = \frac{3}{2}(S_{mm33} - \alpha).$$

Determining s^{B}_{33} from (15), substituting into (19) and dividing by $(1 + \alpha k)$ gives σ^{B}. Stress components perpendicular and parallel to the short axis of the band are given by

$$\sigma^{B}_{33} = \sigma^{B} + s^{B}_{33}$$
$$\sigma^{B}_{11} = \sigma^{B} - s^{B}_{33}/2. \quad (20)$$

The expressions for the stress reduce correctly to the proper results in the limit of a sphere (although this is not a realistic shape for a compaction band). If the shear modulus of the band is finite (neither zero nor unbounded), then expansion of the general expressions for small aspect ratio reveals that the zero aspect ratio limit yields results identical to those for a planar layer considered by Cocco & Rice (2002) and used by Sternlof *et al.* (2005). If the 3-axis is the short axis of the ellipsoid, then Cocco & Rice (2002) noted that $\varepsilon^{B}_{ij} = \varepsilon^{\infty}_{ij}$ if neither i nor j is three and that $\sigma^{B}_{ij} = \sigma^{\infty}_{ij}$ if either i or j is three. The particular relations relevant here are

$$\sigma^{B}_{33} = \sigma^{\infty}_{33} \quad (21a)$$
$$\varepsilon^{B}_{11} = \varepsilon^{\infty}_{11}, \quad \varepsilon^{B}_{22} = \varepsilon^{\infty}_{22}. \quad (21b)$$

Using (21a), and (3) and (2) to eliminate the elastic strains from (21b) yields

$$\sigma^{B}_{11} = \frac{(1+\nu_{B})}{(1-\nu_{B})}\left\{\frac{(1-\nu)}{(1+\nu)}\frac{\mu_{B}}{\mu}\sigma^{\infty}_{11} + \sigma^{\infty}_{33}\left[\frac{\nu_{B}}{(1+\nu_{B})} - \frac{\mu_{B}}{\mu}\frac{\nu}{(1+\nu)}\right] - 2\mu_{B}\varepsilon^{P}_{11}\right\} \quad (22)$$

where $\sigma_{22} = \sigma_{11}$ in both the band and the far field for axisymmetry (identical to equations (4b) and (4c) of Sternlof *et al.* (2005) for axisymmetry and slightly different notation).

If the shear modulus is zero, then the band reduces to a void and the stresses in the band are zero. In the limit of the short axis of the ellipsoid, c, approaching zero, the products of c and the strains ε^{B}_{3j} equal the crack (or anti-crack) surface displacements predicted by fracture mechanics (Rudnicki 1977; Hoenig 1978). In the case of compressive loading the crack surfaces are predicted to interpenetrate. This analogue of a tensile crack with the signs of the stresses and displacements reversed has been termed an 'anti-crack' (Fletcher & Pollard 1981) and applied to compaction bands by Sternlof & Pollard (2002) and Sternlof *et al.* (2005). In the application to compaction bands, this interpenetration is interpreted as inelastic compaction of a narrow, but finite width band.

If the shear modulus of the band is unbounded, then the ellipsoid is rigid and has a shape change specified by ε^{p}_{mn} (without alteration by the constraint of the matrix). In the limit of the short axis of the ellipsoid, c, approaching zero, the products of c and the strains ε^{p}_{3j} become equal to the specified relative displacements (which are interpenetration for a compaction band), as in a dislocation (or anti-dislocation) model (Katsman *et al.* 2006). Hence, the Eshelby inclusion model encompasses both a crack (or anti-crack) and a dislocation (or anti-dislocation) in the limits of a vanishingly thin zone and either zero or unbounded moduli.

Typically, the aspect ratio, $e = c/a$, of compaction bands is very small. Values from data of Sternlof *et al.* (2005) range from 10^{-3} to 10^{-4} and, consequently, those workers argued that the zero aspect ratio limit is a good approximation. Here we will provide additional quantitative support for this approximation and extend the conditions for which it applies by comparing the results for the zero aspect ratio limit with those obtained using the general expressions for a flat, but finite aspect ratio axisymmetric ellipsoid.

Figure 2 plots the stress normal to the plane of the band σ^{B}_{33}, divided by σ^{∞}_{33}, the far-field normal stress, and Figure 3 plots the stress parallel to the plane of the band σ^{B}_{11}, divided by σ^{∞}_{33}, against the aspect ratios ranging from 10^{-4}–10^{-1} for fixed values of other parameters. The other parameters are varied about a set similar to those inferred by Sternlof *et al.* (2005) for the Valley of Fire. These are only the normal inelastic strain ε^{p}_{33} nonzero, identical elastic constants for the band and matrix, $\mu_{B} = \mu$ and $\nu_{B} = \nu = 0.2$, lateral far-field stress equal to half the normal stress (i.e. $\sigma^{\infty}_{11} = \sigma^{\infty}_{22} = 0.5\sigma^{\infty}_{33}$) and the ratio $\sigma^{\infty}_{33}/2\mu\varepsilon^{p}_{33}$ equal to 0.05.

Figures 2a and 3a show the effect of varying the ratio $\sigma^{\infty}_{33}/2\mu\varepsilon^{p}_{33}$ on $\sigma^{B}_{33}/\sigma^{\infty}_{33}$ and $\sigma^{B}_{11}/\sigma^{\infty}_{33}$. Sternlof

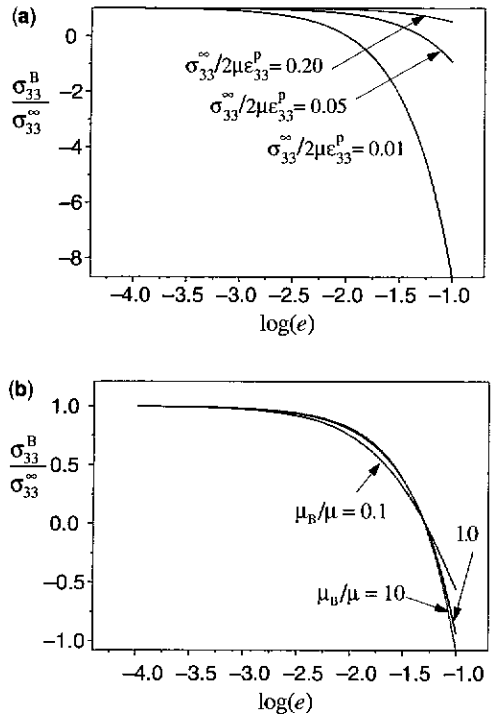

Fig. 2. Stress normal to the plane of the band σ^B_{33}, divided by σ^∞_{33}, the far-field normal stress, against aspect ratios ranging from 10^{-4} to 10^{-1}. (**a**) Results for three values of $\sigma^\infty_{33}/2\mu\varepsilon^p_{33}$ and fixed values of other parameters: $\varepsilon^p_{11} = \varepsilon^p_{22} = 0$, $\mu_B = \mu$, $\nu_B = \nu = 0.2$, and $\sigma^\infty_{11} = \sigma^\infty_{22} = 0.5\sigma^\infty_{33}$. (**b**) Results for $\sigma^\infty_{33}/2\mu\varepsilon^p_{33} = 0.05$ and three values of μ_B/μ with other parameters the same as in (a).

et al. (2005) used $\varepsilon^p_{33} = 0.1$, corresponding to a roughly 10% porosity loss in the band. For the value of Young's modulus $E = 20$ GPa and Poisson's ratio $\nu = 0.2$ estimated by Sternlof *et al.* (2005), the corresponding shear modulus is $\mu = 8.3$ GPa. Their best estimate of the maximum principal compressive stress at the time of band formation was 40 MPa, although they noted a possible range of 13–54 MPa. For $\sigma^\infty_{33} = 40$ MPa the ratio $\sigma^\infty_{33}/2\mu\varepsilon^p_{33}$ is about 0.02, and Figures 2a and 3a show results for the values 0.01, 0.05, and 0.20. For aspect ratios less than about $10^{-2.5}$, the results from (21a) and (21b), corresponding to $\sigma^B_{33} = \sigma^\infty_{33}$ and $\sigma^B_{11} = \sigma^\infty_{11}$, are a very good approximation. The approach to this limit is slower for larger values of ε^p_{33}. Nevertheless, the ratio $\sigma^\infty_{33}/2\mu\varepsilon^p_{33}$ would have to be much smaller for there to be any significant deviation from the zero aspect ratio limit in the range of aspect ratios reported by Sternlof *et al.* (2005). It is, however, interesting to note that the signs of σ^B_{11} and σ^B_{33} differ from that of σ^∞_{33} for larger aspect ratios and the value at which the change of sign occurs decreases with decreasing $\sigma^\infty_{33}/2\mu\varepsilon^p_{33}$. This occurs because of competition between the effects of the far-field compressive stress and the inelastic compaction. If inelastic compaction occurred in the absence of far-field stress, the stresses in the band would need to be tensile for the total band deformation to be compatible with the matrix. This effect is, however, countered by the effect of the far-field compressive stress, which is amplified as the aspect ratio of the band decreases.

A 10% porosity loss in the band, corresponding to $\varepsilon^p_{33} = 0.1$, is also representative of compaction bands formed in axisymmetric compression experiments (Olsson 1999; Olsson & Holcomb 2000; Wong *et al.* 2001; Holcomb & Olsson 2003; Baud *et al.* 2004; Fôrtin *et al.* 2006), although there is some evidence in Castlegate sandstone (Olsson 1999; Olsson & Holcomb 2000; Holcomb & Olsson 2003) that the compaction is not purely uniaxial and that $\varepsilon^p_{11} = \varepsilon^p_{22}$ is extensile (dilatant) (D. Holcomb, pers. comm.). Whether this is a general feature of band formation or is due to the limited lateral constraint in the laboratory is not clear. Values of the axial stress at which compaction bands form in the laboratory tend to be much higher than the 13–54 MPa estimated by Sternlof *et al.* (2005) for field conditions at the time of band formation in the Valley of Fire. Typically, the axial stress at band formation in the laboratory ranges from more than 100 MPa (e.g. Olsson & Holcomb 2000) to several hundred MPa (e.g. Baud *et al.* 2004). Estimates of the shear modulus from axial stress v. strain curves of Olsson & Holcomb (2000) and Baud *et al.* (2004) yield values in the range of 5–10 GPa, similar to that estimated from Sternlof *et al.* (2005). Thus, the ratio $\sigma^\infty_{33}/2\mu\varepsilon^p_{33}$ appropriate for laboratory conditions may be *c.* 2–10 times larger than estimated from Sternlof *et al.* (2005).

Figures 2b and 3b show the effect of decreasing and increasing the band shear modulus by a factor of 10 (in Fig. 3b the zero aspect ratio limit is shown by a dashed horizontal line). The effect on σ^B_{33} is small and the effect on σ^B_{11} corresponds well to the prediction of equation (22) for aspect ratios less than $10^{-2.5}$. Figure 3(c and d) shows that variation of σ^B_{11} as a result of changes in the band Poisson's ratio and the lateral far-field stress are also predicted well by equation (22) for small aspect ratios. Changing these parameters has virtually no effect on σ^B_{33} and, hence, is not shown.

These results confirm that the simplified layer solution, analogous to that of Cocco & Rice (2002) and used by Sternlof *et al.* (2005), is

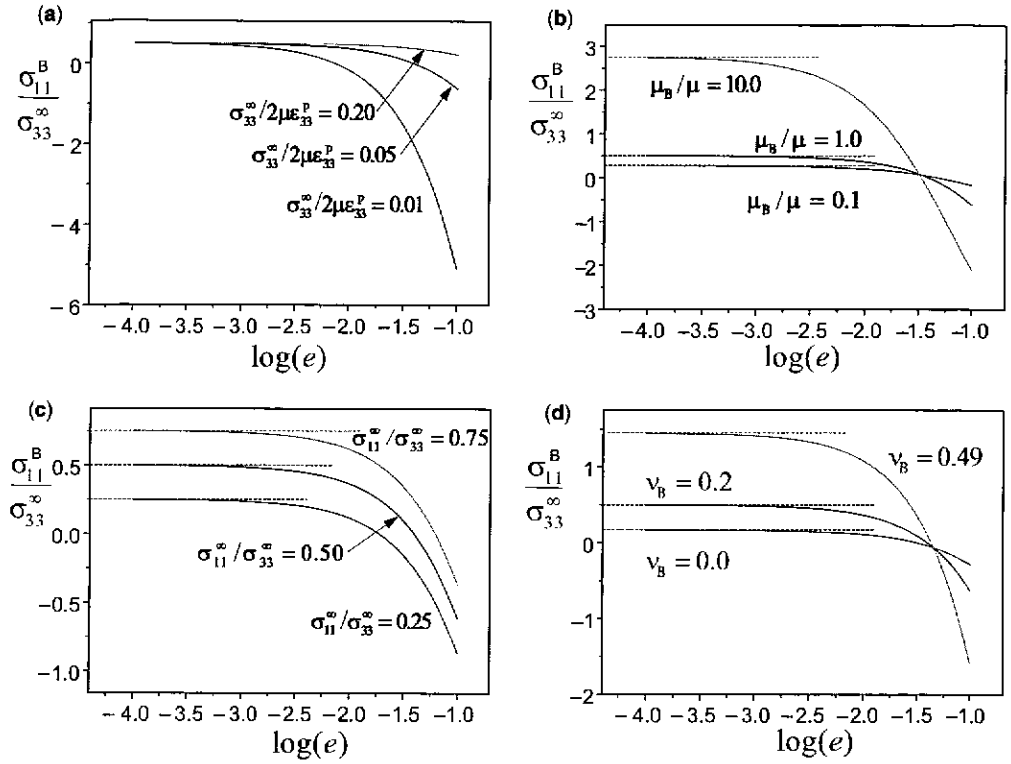

Fig. 3. Stress parallel to the plane of the band σ^B_{11}, divided by σ^∞_{33}, against the aspect ratios ranging from 10^{-4} to 10^{-1} for fixed values of other parameters: $\varepsilon^p_{11} = \varepsilon^p_{22} = 0$, $\mu_B = \mu$, $\nu_B = \nu = 0.2$, $\sigma^\infty_{11} = \sigma^\infty_{22} = 0.5\sigma^\infty_{33}$ and $\sigma^\infty_{33}/2\mu\varepsilon^p_{33} = 0.05$. (**a**), (**b**), (**c**) and (**d**) show the effects of changing $\sigma^\infty_{33}/2\mu\varepsilon^p_{33}$, μ_B/μ, $\sigma^\infty_{11}/\sigma^\infty_{33}$ and ν_B, respectively.

indeed a good approximation for the very small aspect ratios that have been observed, but there is no impediment to similar calculations for larger aspect ratios. Therefore, in the next section we will adopt this approximation and examine the effects of elastic property mismatch, far-field stress ratio and inelastic compactive strain on the stress state immediately adjacent to the band.

Stress state adjacent to the band

The stress immediately outside the band can be obtained from conditions of continuity of traction and displacement across the band–matrix interface. If, as depicted in Figure 1, the midplane of the ellipsoid lies in the x_1x_2-plane and the short axis is in the x_3 direction, then continuity of normal traction on the x_1-axis requires

$$\sigma^{tip}_{11} = \sigma^B_{11}. \tag{23}$$

Continuity of displacement requires that $u^{tip}_2 = u^B_2$ and $u^{tip}_3 = u^B_3$. Consequently, the derivatives tangent to the band–matrix boundary must also be continuous, requiring that

$$\varepsilon^{tip}_{22} = \varepsilon^B_{22}, \quad \varepsilon^{tip}_{33} = \varepsilon^B_{33}. \tag{24}$$

Using the elasticity relations (2) and (3) to eliminate the strains gives

$$\sigma^{tip}_{22} = \frac{\mu}{\mu_B}\sigma^B_{22} + \frac{\nu}{(1-\nu)}\sigma^B_{11}\left(1 - \frac{\mu}{\mu_B}\right) + \frac{\mu}{\mu_B}\sigma^B_{kk}\frac{\nu - \nu_B}{(1-\nu)(1+\nu_B)} + \frac{2\mu}{(1-\nu)}\left(\varepsilon^p_{22} + \nu\varepsilon^p_{33}\right) \tag{25a}$$

$$\sigma^{tip}_{33} = \frac{\mu}{\mu_B}\sigma^B_{33} + \frac{\nu}{(1-\nu)}\sigma^B_{11}\left(1 - \frac{\mu}{\mu_B}\right) + \frac{\mu}{\mu_B}\sigma^B_{kk}\frac{\nu - \nu_B}{(1-\nu)(1+\nu_B)} + \frac{2\mu}{(1-\nu)}\left(\varepsilon^p_{33} + \nu\varepsilon^p_{22}\right) \tag{25b}$$

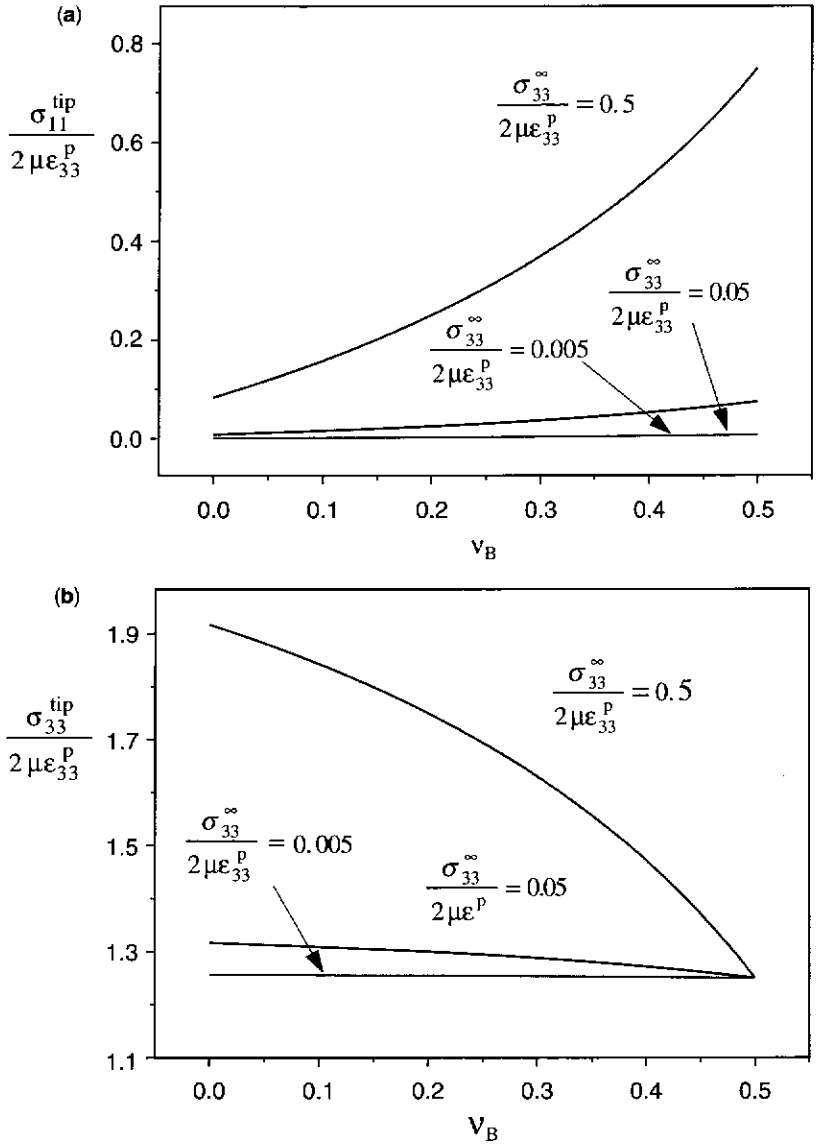

Fig. 4. Stress components σ_{33}^{tip} (**b**) and σ_{11}^{tip} (**a**), divided by $2\mu\varepsilon_{33}^{p}$, against the band Poisson's ratio ν_B for values of $\sigma_{33}^{\infty}/2\mu\varepsilon_{33}^{p}$ an order of magnitude smaller (0.005) and larger (0.5) than for the base set (0.05). Other parameters are $\varepsilon_{11}^{p} = \varepsilon_{22}^{p} = 0$, $\nu = 0.2$, $\mu_B = \mu$, and $\sigma_{11}^{\infty} = \sigma_{22}^{\infty} = 0.5\sigma_{33}^{\infty}$.

which are the same as equations (6) of Sternlof *et al.* (2005) (with slightly different notation). It should be noted that even if the ellipsoid and far-field stress state are axisymmetric, the stress state adjacent to the band is not. Because the localization criterion for compaction band formation (Issen & Rudnicki 2000) indicates that axisymmetric compression stress states are most favourable, the departure from axisymmetry would diminish the tendency for localization.

The relations (23) and (24) will hold at any point adjacent to the band if expressed in terms of the local normal and tangent directions. In particular, we note that the conditions at the flank of the

band (on the x_3-axis at the band boundary; see Fig. 1) are

$$\sigma_{33}^{\text{flank}} = \sigma_{33}^{\text{B}} \tag{26a}$$

$$\varepsilon_{22}^{\text{flank}} = \varepsilon_{22}^{\text{B}}, \quad \varepsilon_{11}^{\text{flank}} = \varepsilon_{11}^{\text{B}}. \tag{26b}$$

These equations, together with equation (21), imply that for a thin (zero aspect ratio) band, the stress state at the flank is identical to that in the far field.

Similarly to the procedure in the preceding section, we will explore the effect of altering parameters on the stress state adjacent to the band for variations about a base set of parameters. This base set is only $\varepsilon_{33}^{\text{p}} \neq 0$ ($\varepsilon_{11}^{\text{p}} = \varepsilon_{22}^{\text{p}} = 0$), Poisson's ratio of the matrix $\nu = 0.2$, equal shear moduli for band and matrix, $\mu_{\text{B}} = \mu$, lateral far-field stress equal to half the normal stress, $\sigma_{11}^{\infty} = \sigma_{22}^{\infty} = 0.5\sigma_{33}^{\infty}$, and $\sigma_{33}^{\infty}/2\mu\varepsilon_{33}^{\text{p}} = 0.05$. Components of the stress in the band, divided by $2\mu\varepsilon_{33}^{\text{p}}$, are plotted against ν_{B}, the Poisson's ratio in the band. For $\mu_{\text{B}} = \mu$, and $\nu = 0.2$, $\nu_{\text{B}} = 0$ corresponds to $\kappa_{\text{B}}/\kappa = 0.5$; for $\kappa_{\text{B}}/\kappa = 2, 3, 5, 10$, the corresponding values of ν_{B} are 0.333, 0.385, 0.429 and 0.463, respectively. Because the porosity of the band material is reduced relative to the matrix, it is likely that the bulk modulus of the band material will exceed that of the matrix $\kappa_{\text{B}}/\kappa > 1$, but there are no quantitative estimates. Plotting results against ν_{B} covers the entire range of possibilities.

Figure 4 shows σ_{33}^{tip} and σ_{11}^{tip} for values of $\sigma_{33}^{\infty}/2\mu\varepsilon_{33}^{\text{p}}$ an order of magnitude smaller (0.005) and larger (0.5) than for the base set (0.05). Values of $\sigma_{22}^{\text{tip}}/2\mu\varepsilon_{33}^{\text{p}}$ do not depend on ν_{B} and equal 0.253, 0.275 and 0.5 for $\sigma_{33}^{\infty}/2\mu\varepsilon_{33}^{\text{p}} = 0.005$, 0.05, and 0.5, respectively. Only for $\sigma_{33}^{\infty}/2\mu\varepsilon_{33}^{\text{p}} = 0.5$ and small ν_{B} does $\sigma_{33}^{\text{tip}}/2\mu\varepsilon_{33}^{\text{p}}$ rise significantly above unity (to about 1.9 for $\nu_{\text{B}} = 0$) and only for $\sigma_{33}^{\infty}/2\mu\varepsilon_{33}^{\text{p}} = 0.5$ and large ν_{B} does $\sigma_{11}^{\text{tip}}/2\mu\varepsilon_{33}^{\text{p}}$ depart significantly from zero (to about 0.8 for $\nu_{\text{B}} = 0.5$). The ratio $\sigma_{33}^{\infty}/2\mu\varepsilon_{33}^{\text{p}} = 0.5$ corresponds to a relatively small compactive strain or relatively large far-field compressive stress normal to the plane of the band.

Figure 5 shows the effect of uniaxial ($\sigma_{11}^{\infty}/\sigma_{33}^{\infty} = 0.0$) and hydrostatic ($\sigma_{11}^{\infty}/\sigma_{33}^{\infty} = 1.0$) far-field stress in addition to the base value $\sigma_{11}^{\infty}/\sigma_{33}^{\infty} = 0.5$. The stress σ_{33}^{tip} increases with increasing triaxiality ($\sigma_{11}^{\infty}/\sigma_{33}^{\infty}$) for $\nu_{\text{B}} < \nu$ and decreases with increasing triaxiality for $\nu_{\text{B}} > \nu$. The stress σ_{11}^{tip} increases with triaxiality and ν_{B} but, again, the variation is small (*c.* $0.1 \times 2\mu\varepsilon_{33}^{\text{p}}$). The stress component σ_{22}^{tip} is again independent of ν_{B} and equal to 0.25, 0.275 and 0.30 multiplied by $2\mu\varepsilon_{33}^{\text{p}}$ for $\sigma_{11}^{\infty}/\sigma_{33}^{\infty} = 0.0$, 0.5 and 1.0. An interesting feature of Figure 5b is that for $\sigma_{11}^{\infty}/\sigma_{33}^{\infty} = 0$, σ_{11}^{tip} is negative (tensile) for $\nu_{\text{B}} < \nu$ and positive (compressive) for $\nu_{\text{B}} > \nu$, although the magnitude is small.

Figure 6 shows the effect of a band shear modulus that is an order of magnitude larger or smaller than the matrix modulus. Although, as argued above, it is likely that the bulk modulus of the band will exceed that of the matrix, the relative size of the shear moduli is not so clear. Greater density (as a result of decrease of porosity) might increase the shear modulus. More likely, decohesion and, sometimes, fragmentation of the band material would reduce the resistance to shear by facilitating particle rearrangement and rolling. Decreasing the ratio of the shear moduli to $\mu_{\text{B}}/\mu = 0.1$ increases σ_{33}^{tip}, except for ν_{B} near 0.5. The effect is greatest for small values of ν_{B} but the maximum increase is less than a factor of two. The variation of σ_{22}^{tip} with ν_{B} is similar for $\mu_{\text{B}}/\mu = 0.1$, although the magnitude of the increase for a reduced shear modulus is smaller than for σ_{33}^{tip}. Although a value of band shear modulus much greater than the matrix modulus seems unlikely, the stresses are shown for $\mu_{\text{B}}/\mu = 10.0$. The increase in the ratio of shear modulus from one to 10 has little effect on σ_{33}^{tip}, reduces σ_{22}^{tip} slightly, more so for ν_{B} near 0.5, and increases σ_{11}^{tip} from very small fractions of $2\mu\varepsilon_{33}^{\text{p}}$ to $0.1-0.32\mu\varepsilon_{33}^{\text{p}}$.

In summary, for a wide variation of parameters about the base set, σ_{33}^{tip} is about 1–2 times $2\mu\varepsilon_{33}^{\text{p}}$. The other stress components are typically around a few tenths to half of σ_{33}^{tip}. These results suggest that the stress state at the band tip is mainly controlled by $2\mu\varepsilon_{33}^{\text{p}}$ rather than the far-field stress, unless its magnitude is comparable with $2\mu\varepsilon_{33}^{\text{p}}$.

Energy release propagation criterion

The results of the preceding section have shown that when the aspect ratio of the bands is of the order of the values inferred from field observations by Sternlof *et al.* (2005), $10^{-3}-10^{-4}$, the actual value of the aspect ratio has little effect on the stress state at the band tip and can be taken as zero. Similarly, if the inelastic compactive strain $\varepsilon_{33}^{\text{p}} = 0.1$ and the ratio of the matrix shear modulus to remote stress (normal to the band) is of the order of 10^2, even implausibly large variations of the contrast of elastic moduli have relatively little effect. In short, the ratio of the stress at the tip of the band to that in the far field is in the range 10–100 and is controlled primarily by the product of the magnitude of the inelastic compactive strain and the ratio of the shear modulus to remote stress. The ratio of stress at the tip of the band to remote stress does, however, increase with a reduction in the band

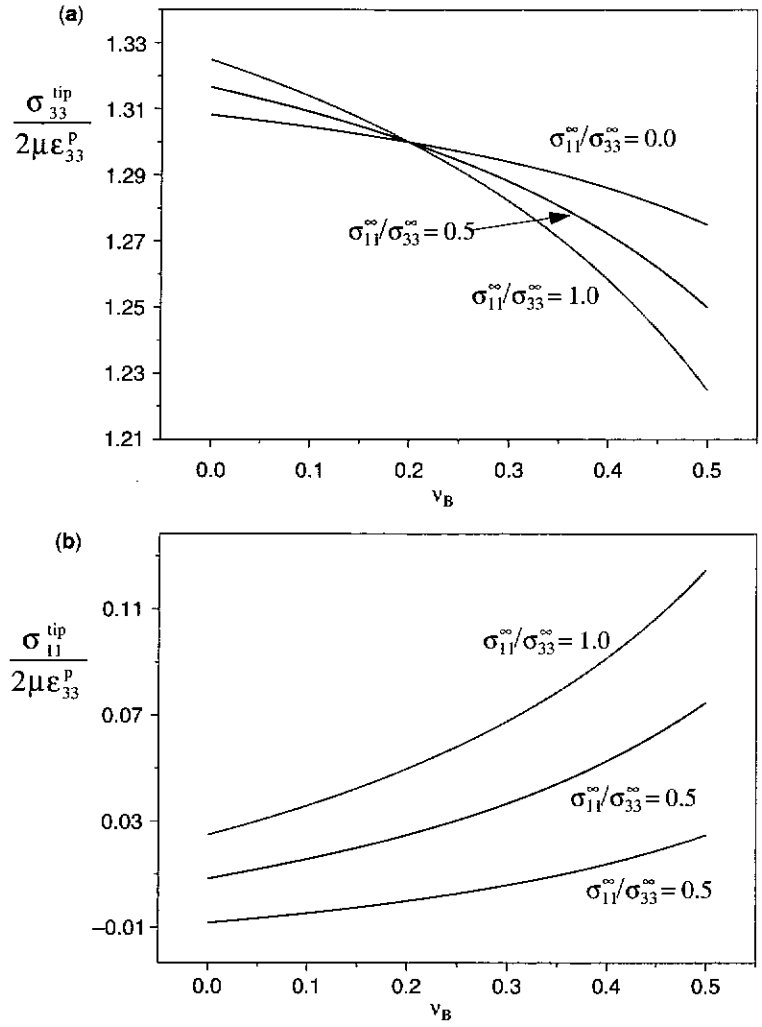

Fig. 5. Same as Figure 4 but with $\sigma_{33}^{\infty}/2\mu\varepsilon_{33}^{p} = 0.05$ and $\sigma_{11}^{\infty}/\sigma_{33}^{\infty} = 0.0$, 0.5 and 1.0.

shear modulus and becomes unbounded in the limit $\mu_B \to 0$. The inferred level of stress elevation, 10–100 times the far-field stress, is consistent with the concept that band propagation occurs in a crack-like manner.

Although these results demonstrate that the normal stress just ahead of a compaction band is elevated, they give no indication of what level is needed for propagation. As the bands observed in the field have stopped propagating, we can only say that the current level is below that needed for propagation. A useful approach to the condition for propagation is to consider the energy released per unit band extension, as has been successfully applied to tensile and shear fractures. Vajdova & Wong (2003) and Tembe *et al.* (2006) have used this approach to interpret the extension of compaction bands from circumferentially notched specimens of Bentheim and Berea sandstone. By estimating the compaction energy from the nominal stress v. displacement curves, Vajdova & Wong (2003) obtained a lower bound on the compaction energy for Bentheim sandstone of 16 kJ m^{-2} and Tembe *et al.* (2006) estimated values ranging from 6 to 43 kJ m^{-2} for Berea and Bentheim sandstones.

Rudnicki & Sternlof (2005) have developed the idea for compaction energy release using a simple model adapted from an example used by Rice (1968*a*) to illustrate the *J*-integral. They considered a long (semi-infinite) compaction band in an infinite

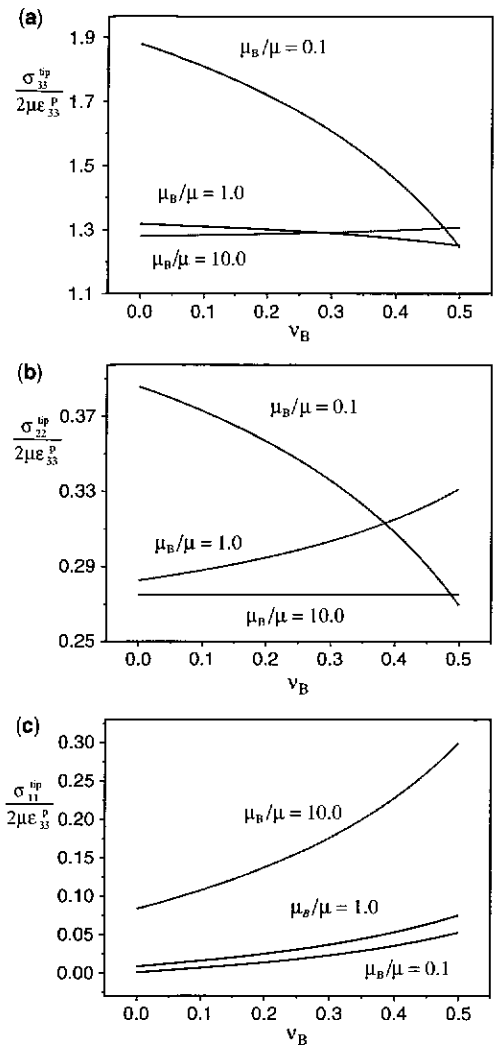

Fig. 6. Same as Figure 4 but with $\sigma_{33}^{\infty}/2\mu\varepsilon_{33}^{P} = 0.05$ and $\mu_B/\mu = 0.1$, 1.0 and 10.0 and also showing $\sigma_{22}^{\infty}/2\mu\varepsilon_{33}^{P}$ (**b**).

strip of width w (taken as representative of the distance between bands in application to the field data) with an elastic modulus for 1D strain of M $(=2\mu(1-\nu)/(1-2\nu)$ for an isotropic elastic material). The compaction band attains a constant thickness ξw far behind its tip where the elastic modulus in the band is M_B and the 1D inelastic compactive strain is ε^P. Because the configuration is translationally invariant in the direction of the band and strip, advance of the band a unit distance reduces the strain energy of a vertical slice of material far ahead of the band tip to that of a vertical slice far behind the band tip. Rudnicki & Sternlof (2005) gave an exact result for this difference, but if the band thickness is very much less than w, $\xi \ll 1$, and the band modulus does not differ significantly from the modulus of the surrounding material, the energy release is given by the simple expression

$$\mathcal{G}_{\text{band}} = \sigma_+ \xi \varepsilon^P w \tag{27}$$

to first order in ξ. In equation (27), $\sigma_+ = M(\Delta/w)$ is the uniform compressive stress far ahead of the band tip and Δ is the relative closure of the layer boundaries (so that Δ/w is the nominal strain in the absence of the band). Thus, the energy released (per unit area of band advance) has the interpretation of the stress multiplied by the compactive displacement in the band. For representative values of the parameters derived for the Aztec sandstone corresponding to 1 cm thick compaction bands spaced 1 m apart, and $\varepsilon^P = 0.1$, corresponding to a porosity reduction of 10%, Sternlof *et al.* (2005) found $\mathcal{G}_{\text{band}} = 40\ \text{kJ m}^{-2}$. This result is surprisingly similar to the range of compaction energies estimated by Vajdova & Wong (2003) and Tembe *et al.* (2006) for different sandstones and laboratory conditions.

Combined anti-crack–dislocation model

As discussed above, the data on compaction band profiles from the Valley of Fire (Sternlof *et al.* 2005) are nearly elliptical. The ratio of midpoint thickness to band length is not, however, constant as would be the case for self-similar ellipses (or as predicted for the ratio of midpoint displacement to length for an anti-crack model with uniform surface tractions). Sternlof *et al.* (2005, Fig. 4b) showed that the midpoint thickness increases more slowly for the longer bands. For the shorter bands (less than about 10 m), the half-width increases roughly linearly with length. This suggests the possibility of self-similar extension, although the aspect ratios are so small that any lateral spreading must also be small. The widths of the three longest bands do not follow this trend but increase with length at a smaller rate. Sternlof (2006) suggested that the midpoint thickness reaches an asymptotic value for the longest bands, although the data are not unambiguous on this issue because of the difficulty of identifying very long, isolated bands. He suggested a conceptual model (see his fig. 4.23) that is similar to the simple plane strain (infinite in extent out of the plane of the sketch) model shown in Figure 7.

This configuration is identical to that for a tensile solution given by Tada *et al.* (1973) with the signs of the stress and displacement reversed.

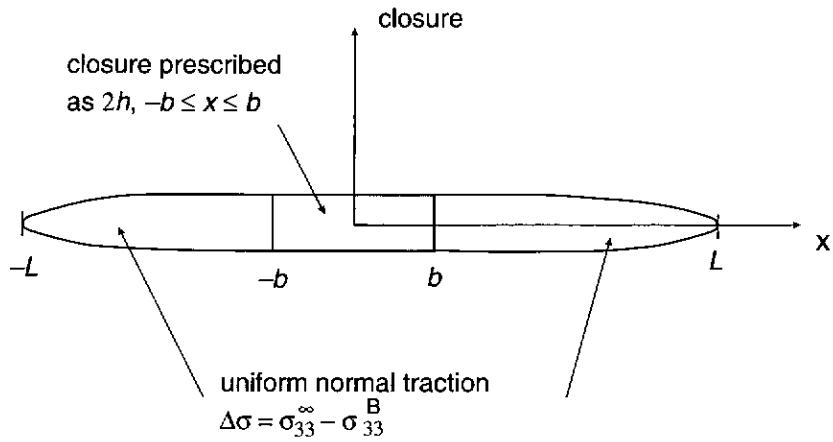

Fig. 7. Schematic illustration of a compaction band of total length $2L$. A uniform compactive displacement $2h$ is specified for $-b \leq x \leq b$ and a uniform closure traction, equal to the difference between the far-field compressive stress σ_{33}^{∞} and the resistive stress in the band σ_{33}^{B}, is specified for $|b| < x \leq |L|$. This is a plane strain model and, hence, extends indefinitely out of the plane of the sketch. Displacements are shown as opening for clarity but correspond to interpenetration (compaction) in the model.

(Again the interpenetration of the crack surfaces is interpreted as inelastic compactive displacement.) The compaction band has total length $2L$ with a uniform compactive displacement $2h$ specified for $-b \leq x \leq b$. For $|b| < |x| \leq |L|$ a uniform closure traction, equal to the difference between the far-field compressive stress σ_{33}^{∞} and the resistive stress in the band σ_{33}^{B}, is specified. The magnitude of this traction is chosen to eliminate the singularity in stress at $x = \pm b$, or equivalently, to ensure that the tangent to the profile of crack surface displacements is continuous. This traction is given by

$$\Delta\sigma = \frac{\mu h}{L(1-\nu)} \frac{1}{E_1(k) - (b/L)^2 E_2(k)} \tag{28}$$

where $k = \sqrt{1-(b/L^2)}$ and E_1 and E_2 are the complete elliptic integrals of the first and second kinds, respectively. The stress intensity factor at the ends of the compaction band is given by

$$K = \sqrt{\frac{\pi}{L-b}} \frac{\mu h}{(1-\nu)} \left\{ \frac{k\sqrt{1-b/L}}{E_1(k) - (1-k^2)E_2(k)} \right\}. \tag{29}$$

The factor $\{\ldots\}$ equals unity in the limit $b/L \to 0$ ($k \to 1$). In this limit $\Delta\sigma \to \mu h/L(1-\nu)$ so that the stress intensity factor reduces to $\Delta\sigma\sqrt{\pi L}$, the well-known expression for a crack of length $2L$ loaded by a stress $\Delta\sigma$. In the alternative limit, $b/L \to 1$ ($k \to 0$), $\{\ldots\}$ equals $\sqrt{8}/\pi = 0.90$ and equation (29) reduces to

$$K = \sqrt{\frac{8}{\pi}} \frac{1}{\sqrt{(L-b)}} \frac{\mu h}{(1-\nu)} \tag{30}$$

to first order in $1 - b/L$. Equation (30) is the stress intensity factor at the right end of a crack of length $L - b$ wedged open by a semi-infinite dislocation of magnitude $2h$ at the left end and uniform traction to ensure no singularity at the left end (Tada *et al.* 1973). This is identical to the solution for a crack of length $(L - b)$ enclosing a net entrapped dislocation $2h$ and traction chosen to negate the singularity at the left end (Rice 1968*b*). The traction in this case is $\Delta\sigma \to 2\mu h/\pi(L-b)(1-\nu)$, so that the stress intensity factor is twice that for a crack of length $2(L-b)$ with uniform traction $\Delta\sigma$ and no entrapped dislocation. As is evident from equation (30), the stress intensity factor becomes unbounded as $L \to b$ and so also does the traction required to eliminate the singularity at the edge of the dislocation. This behaviour reflects the stronger stress singularity at the edge of a uniform dislocation (reciprocal of distance from the edge) than at the edge of a crack (reciprocal of the square root of distance from the edge). Figure 8a plots the factor $\{\ldots\}$ against b/L from zero to one (corresponding to k varying over the same range). Figure 8b plots the stress intensity factor from equation (29), divided by $\sqrt{\pi}\mu h/\sqrt{L(1-\nu)}$, against b/L. Also shown is $(1-b/L)^{-1/2}$, the approximate result obtained by setting the

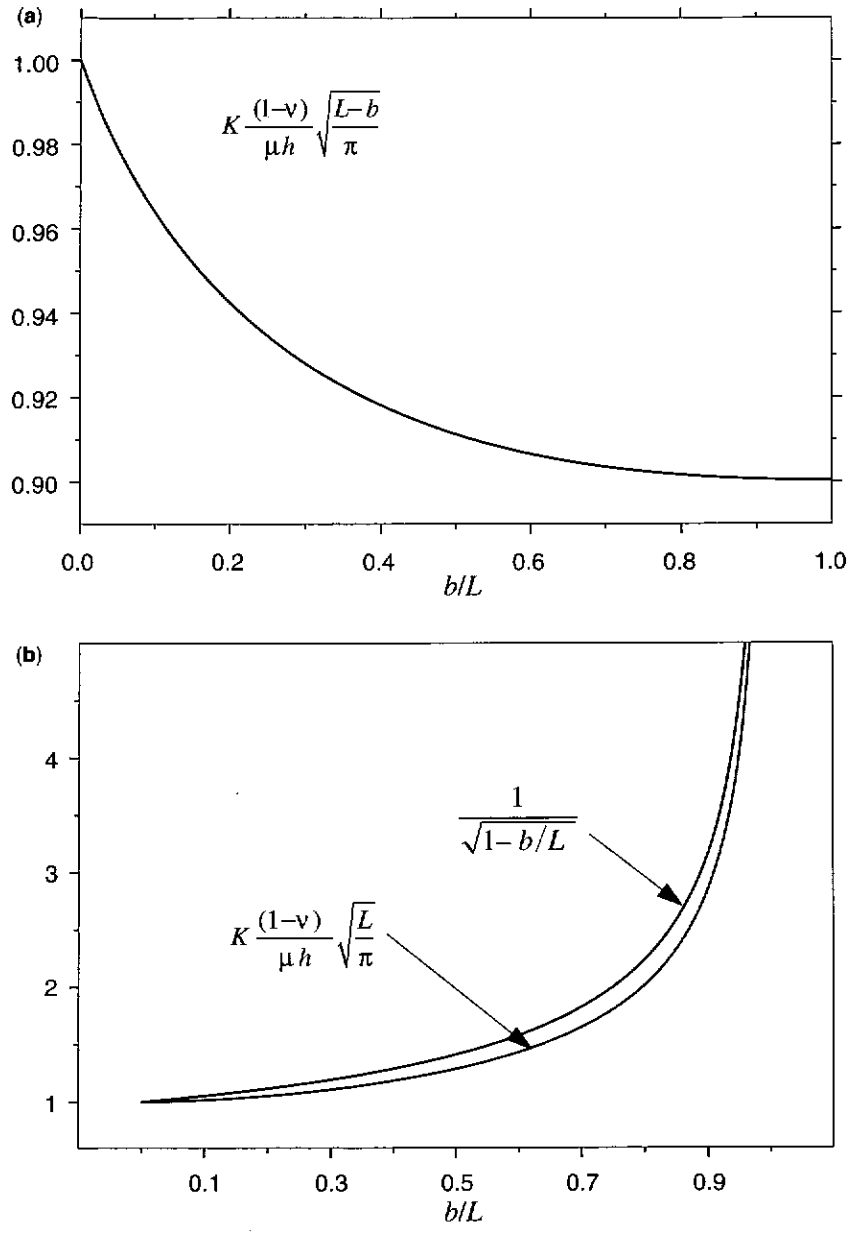

Fig. 8. (a) Plot of the stress intensity factor K at $x_1 = \pm L$ in Figure 7, divided by $\mu h\sqrt{\pi/(L-b)}/(1-\nu)$ against b/L. (b) Comparison of K divided by $\mu h\sqrt{\pi/L}/(1-\nu)$ with $(1-b/L)^{-1/2}$ against b/L.

factor $\{\ldots\}$ in equation (29) equal to unity. As the plot shows, the stress intensity factor is well approximated by

$$K = \sqrt{\frac{\pi}{L-b}}\frac{\mu h}{(1-\nu)} \tag{31}$$

not only near $b/L \to 0$, where it is exact, but over most of the range of b/L.

Tada *et al.* (1973) also gave the expression for the crack surface displacements (here, closure or interpenetration). These are plotted in Figure 9 for b/L equal to 0, 0.25, 0.5, 0.75, and 0.9. For $b/L = 0$, there is no entrapped dislocation and the

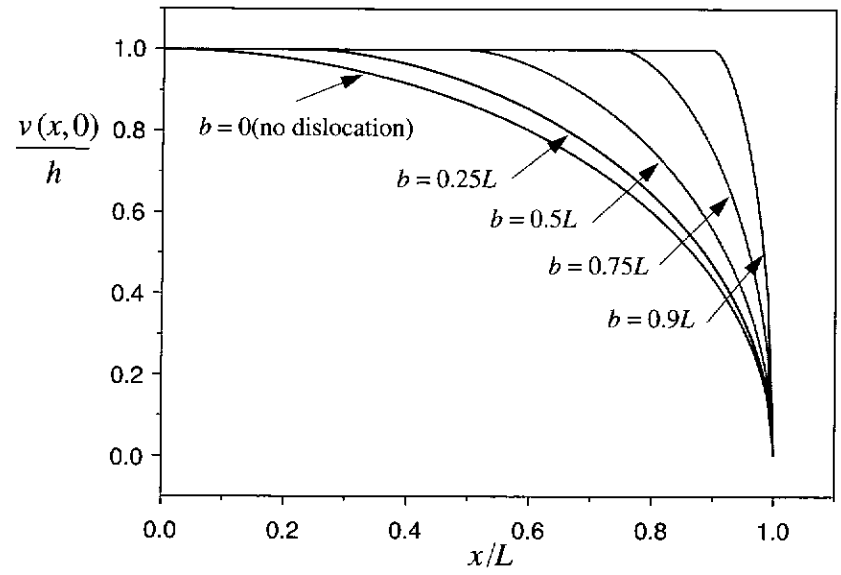

Fig. 9. Closing displacement divided by half the imposed closing dislocation h against distance from the centre divided by the band half-width L. Profiles are plotted for $b/L = 0$, 0.25, 0.5, 0.75 and 0.9.

displacement profile is purely elliptical (as for a crack loaded by uniform surface tractions). As long as b/L is not too large, the profiles do not differ significantly from elliptical and probably fall within the scatter of data from figure 4a of Sternlof *et al.* (2005).

The roughly elliptic displacement profiles measured by Sternlof *et al.* (2005) suggest that b/L is small and the stress intensity factor can be approximated by equation (31) with $b = 0$. Substituting this value into the relation between the stress intensity factor and energy release rate $\mathcal{G}$,

$$\mathcal{G} = (1 - \nu)K^2/2\mu \tag{32}$$

and rearranging yields

$$\frac{2h}{\sqrt{L}} = \sqrt{\frac{8\mathcal{G}(1-\nu)}{\pi\mu}}. \tag{33}$$

Thus, if compaction bands are assumed to grow at a constant, critical value of the energy release rate, equation (33) implies that the band thickness (or midpoint closure) should scale as the square root of the band half-length. This predicted scaling is consistent with a recent analysis of compaction band data by Rudnicki *et al.* (2006). They replotted the data from Figure 4b of Sternlof *et al.* (2005) on a log–log scale, and added several points from laboratory data and from field data of Hill (1989) and Mollema & Antonellini (1996). Fitting a straight line through the data yields a relationship of the form

$$2h = AL^B \tag{34}$$

where A and B are constants. The exponent B is roughly 1/2: 0.42, 0.5, and 0.53 for fitting the entire dataset, all the field data and the Sternlof *et al.* (2005) data, respectively. (Fossen & Hesthammer (1997) have reported a similar scaling relation (width proportional to the square root of length) for deformation bands in Jurassic sandstone in southeastern Utah.) For $\mu = 8.33$ GPa and $\nu = 0.2$, values inferred for the Valley of Fire by Sternlof *et al.* (2005), the coefficient A corresponds to critical values of $\mathcal{G}$ equal to 25, 30, and 37 kJ/m^{-2} for the same three fits. These values are slightly lower than the $\mathcal{G} = 40$ kJ m^{-2} as estimated by Rudnicki & Sternlof (2005) and consistent with laboratory estimates (Vajdova & Wong 2003; Tembe *et al.* 2006). Using the individual values of $2h$ and L with the same values of μ and ν yields critical energy release rates ranging from 4 to 90 kJ m^{-2} for the field data and 71, 105, and 111 kJ m^{-2} for the three laboratory values. It is not surprising that the laboratory values are at the upper end of the range, as the approximation of $b/L \to 0$ is probably not very good for bands

that extend across the entire specimen. Despite the many uncertainties involved in this comparison, the agreement seems too good to be coincidental and suggests that the model depicted in Figure 7 and suggested by Sternlof (2006) has merit.

Discussion

We have modelled a compaction band as a thin ellipsoidal inhomogeneity subjected to an inelastic compactive strain and compressive stresses in the far field. The shape was strongly suggested by field observations of Sternlof *et al.* (2005) and Sternlof (2006) on the Aztec sandstone of the Valley of Fire, Nevada. For a range of parameters encompassing the field data and aspect ratios typical of the field data, 10^{-3}–10^{-4}, the results show that the stress state in the band does not differ significantly from that for zero aspect ratio. The stress state within the band is primarily controlled by the ratio of the far-field compressive stress to twice the shear modulus of the matrix multiplied by the inelastic compactive strain. For the field data, this ratio is about 0.02–0.05, but it may be several times larger for laboratory experiments. For the approximation of a zero aspect ratio band, the stress state at the flank of the band is identical to the far-field stress state. The stress state at the tip of the band is fully 3D (all three principal stresses differ even when the far-field stress, imposed inelastic strain and band shape are axisymmetric). The calculations suggest that the ratio of the compressive stress ahead of the band and normal to the plane of the band to that in the far field is of the order of 10–100. This ratio is not significantly affected by elastic mismatch within even an implausibly wide range, although the ratio does become unbounded in the limit of the band shear modulus going to zero. Hence, elastic mismatch is not likely to be a major factor in compaction band extension. The stress elevation is dominated by the product of the inelastic compactive strain and the ratio of the shear modulus to far-field compressive normal stress.

Sternlof and Pollard (2002) and Sternlof *et al.* (2003) suggested that compaction bands can be modelled as anti-cracks. Anti-cracks are the compressive counterpart of a tensile crack: the stiffness of material in the band is neglected and the band is idealized as negligibly thin. The predicted interpenetration of anti-crack surfaces, although physically unrealistic, is interpreted as closure of the band boundaries as a result of inelastic compaction. The anti-crack approximation arises as a limit of the inhomogeneity model. As noted above, for zero aspect ratio, the compressive stress at the band tip does become unbounded as the shear modulus within the band μ_B goes to zero. The correspondence between a crack with uniform crack-surface tractions and the limit of a flat ellipsoid is well known (Rudnicki 1977; Hoenig 1978). To obtain this limit properly, it is necessary to consider an ellipsoid with small but finite thickness c, in the limit $c \rightarrow 0$ with $c\varepsilon_{33}^{B}$ remaining finite and equal to the relative crack surface displacements.

The calculations here have demonstrated that results for zero aspect ratios differ negligibly from those for the very small aspect ratios typical of field data, 10^{-3}–10^{-4}, and that σ_{33}^{tip} is roughly one to two orders of magnitude larger than σ_{33}^{∞} for the parameters considered here. Furthermore, the results have been shown not to be strongly dependent on the elastic mismatch (which is not well constrained by observation). For these reasons, it is not unreasonable to idealize the ratio $\sigma_{33}^{tip}/\sigma_{33}^{\infty}$ as unbounded, as it is in the limit $\mu_B/\mu \rightarrow 0$ or for an 'anti-crack'. Sternlof *et al.* (2005) used a MATLAB code (provided by P. Sharma of the University of Houston) to compute the variation of stress (σ_{33} in the notation here) with distance from the tip of an ellipsoidal inclusion. They showed (their fig. 15) that for very small distances the stress varies as $r^{-1/2}$, where r is distance from the tip, as it does near the tip of a crack in a linear elastic material, but that the stress at the interface between band and matrix remains finite (as long as the ellipsoid has finite aspect ratio and nonzero modulus). Sternlof *et al.* (2005) concluded that, at least for parameters representative of field data, the difference between the stress fields of the anti-crack and inclusion models is significant only very close to the tip and the anti-crack model is a reasonable approximation. This idealization of a compaction band as an anti-crack makes it possible to take advantage of the body of results for linear elastic fracture mechanics.

On the other hand, Katsman *et al.* (2006) used numerical calculations with a spring-network model and some analytical calculations for a tabular closing mode dislocation to conclude 'that there is little similarity between stress distributions around CBs and cracks (or anticracks as extended from Fletcher & Pollard (1981)' and proposed that compaction bands are better described as 'anti-dislocations'. Their latter conclusion is supported by the results here in the sense that the ratio $\sigma_{33}^{\infty}/2\mu\ \varepsilon_{33}^{p}$ is small, a few per cent, for field data and that the band and near-tip stress are primarily controlled by the inelastic compactive strain ε_{33}^{p}. Thus, the specified inelastic compactive strain imposes a displacement on the band boundaries rather than a traction, as is normally the case in crack problems.

The distinction between crack and dislocation models is not, however, a sharp one given the

well-known connection between them (Bilby & Eshelby 1968). A 'crack' model typically implies that the distribution of crack surface tractions is specified and the relative crack surface displacements are calculated, whereas a 'dislocation' model implies that the relative displacements are specified. Of course, for a distribution of crack surface tractions there is a corresponding distribution of crack surface displacements (dislocation) and vice versa. Although Sternlof *et al.* (2005) referred to their model as an 'anti-crack', they implemented it by specifying the relative crack surface displacements (dislocation) corresponding to the measured width profiles. Because the measured width profiles are elliptic, the resulting crack surface traction is uniform as for a simple crack model. (In this case, the far-field stress of Sternlof *et al.* (2005) should be regarded as the difference between the far-field stress and this uniform traction.)

As already noted, the stress ahead of a crack (or anti-crack) is singular at the tip and varies as $r^{-1/2}$, where r is distance from the tip. The stress at the edge of a uniform tabular dislocation is, however, also singular and, as noted by Katsman *et al.* (2006), varies as r^{-1}. Of course, the stress in any real material cannot be unbounded and will be alleviated by inelastic processes that are neglected in the linear elastic idealization. A more complex and realistic model might specify the relation between the relative displacements and the tractions in such a way as to reflect the inelastic processes at the tip. At present, however, such details are not constrained by observation. The advantage of the crack formulation is that the energy in finite volumes surrounding the tip is bounded. (This is not the case for a uniform tabular dislocation; this feature is reflected in that $K \rightarrow \infty$ in equation (30) when $L \rightarrow b$.) Consequently, a criterion for propagation can be expressed in terms of a critical value of the stress intensity factor (the coefficient of the inverse square root singular stress on the plane ahead of the crack, usually divided by $\sqrt{2\pi}$) or the energy released per unit area of band advance. In addition, a large body of evidence in fracture mechanics (e.g. Rudnicki 1980; Anderson 1995; Lawn 1983) has established that whenever the actual inelastic processes that occur in response to the high stress at the tip take place in a zone having a length scale much smaller than geometric lengths in the problem (small-scale yielding), the singular elastic field is a good description at distances several times the inelastic process zone size. In this sense, the stress intensity factor (or energy release rate) relates the intensity of the near tip field to the applied loads or displacements in a way that is insensitive to the detailed inelastic processes near the tip. The energy release model of Rudnicki & Sternlof (2005) takes advantage of these features of linear elastic fracture mechanics to compare an estimate of critical energy release rate with values inferred from laboratory tests (Vajdova & Wong 2003; Tembe *et al.* 2006). Similarly, the combined anti-crack–dislocation model discussed here uses the estimated energy release rate to suggest an explanation for the variation of band width with length noted by Sternlof (2006) and elaborated by Rudnicki *et al.* (2006).

The variation and magnitude of the stress field near the band tip will, of course, depend on the inelastic microstructural processes that occur there, including grain decohesion and rearrangement and, possibly, cracking and fracture, as well as the elastic mismatch. If the band is modelled as having a finite stiffness (elastic constants), then it seems unlikely that the stress field will be dramatically altered by variations in the tip shape (as long as there are no corners or vertices, which would be expected to introduce weak singularities). If, however, the band stiffness is neglected and the band is assumed to be very narrow, then the stress at the band tip is approximately inversely proportional to the root radius of the band tip. An elliptical profile of displacements is associated with the inverse square root of distance singularity characteristic of linear elastic fracture mechanics and implies a very small inelastic process zone. The field observations of Sternlof *et al.* (2005) and Sternlof (2006) gave little or no indication of such a process zone at the band tip; their band profiles appeared to be very nearly elliptical as the end is approached. Nevertheless, there is likely to be increased uncertainty in measurements very close to the tip. On the other hand, Tembe *et al.* (2006) used microstructural observations to inelastic process zone sizes of 0.3–0.5 times the notch depth (2 mm) for samples with diameters of 18.4 mm and found that this agrees with predictions of a linear elastic fracture model. The implications of this for the different rock type, stress level and geometry of the field data are not clear, but further information on the details of the compaction processes near the tip of a band would provide insight into the interpretation of the critical energy release rate and its possible dependence on microstructural parameters.

Conclusion

We have used results from Eshelby (1957) to examine the stress state within and at the tip of a compaction band modelled as a thin, ellipsoidal inhomogeneity subjected to an inelastic compactive strain. For parameter values inferred for the field site of Sternlof *et al.* (2005), the compressive stress normal to the plane of the band just ahead

of the tip is of the order of 10–100 times the remote stress. Aspect ratios typical of field data, 10^{-3}–10^{-4}, do not yield results significantly different from those for zero aspect ratio. Elastic mismatch between the band and the surrounding material has only a small effect on the stress ahead of the band for compactive strains, moduli and stresses typical of field values. The relatively minor effect of the elastic mismatch is also consistent with the results of an energy release model of propagation introduced by Rudnicki & Sternlof (2005). This model suggests the product of the remote stress and the relative inelastic compactive displacement as a quantity critical for propagation. An estimate for this product from the field data of Sternlof *et al.* (2005) yields a value of about 40 kJ m^{-2}, similar to values of compaction energies inferred from laboratory tests on circumferentially notched compression samples (Vajdova & Wong 2003; Tembe *et al.* 2006). A combined anti-crack–dislocation model yields quantitative results of the stress intensity factor and the closure distribution for a conceptual model proposed by Sternlof (2006). If the band is assumed to grow at a critical value of the energy release rate estimated by Rudnicki & Sternlof (2005) then the prediction of the variation of band width with length agrees well with that identified by Rudnicki *et al.* (2006).

Principal financial support for this work was provided by the US Department of Energy, Office of Basic Energy Science, Geosciences Research Program through grant DE-FG02-93ER14344/A016 to Northwestern University. I am grateful to K. Sternlof for many helpful discussions and explanations of the field observations, and to S. Tembe and T.-F. Wong for providing their extension and reanalysis of Sternlof's data and for many discussions.

Appendix

The Eshelby factors appearing in equations (15), (16) and (17) of the text are given by

$$S_{3333} = 1 - \frac{(1-2\nu)}{2(1-\nu)} I(e) - \frac{e^2(2-3I(e))}{2(1-\nu)(1-e^2)}$$

$$S_{kk33} = 1 - \frac{(1-2\nu)}{(1-\nu)} I(e)$$

$$S_{33kk} = \frac{(1+\nu)}{(1-\nu)} (1 - I(e))$$

where

$$I(e) = \frac{e}{(1-e^2)^{3/2}} \left\{ \arccos(e) - e(1-e^2)^{1/2} \right\}$$

and, for axisymmetry, the indices '22' can be replaced by '11' wherever they appear. The expression for $I(e)$ corrects a misprint in Rudnicki (2002), which has e^2 instead of e in the numerator of the first term multiplying $\{\ldots\}$. The factor S_{3311} can be determined from

$$S_{3311} = \frac{1}{2}(S_{33kk} - S_{3333})$$

again noting that $S_{3311} = S_{3322}$. S_{1133} can be calculated in similar fashion.

References

ANDERSON, T. L. 1995. *Fracture Mechanics, Fundamentals and Applications*, 2nd edn. CRC Press, Boca Raton, FL.

ANTONELLINI, M. & AYDIN, A. 1994. Effect of faulting on fluid flow in porous sandstones: petrophysical properties. *AAPG Bulletin*, **78**, 355–377.

ANTONELLINI, M. & AYDIN, A. 1995. Effect of faulting on fluid flow in porous sandstone: geometry and spatial distribution. *AAPG Bulletin*, **79**, 642–671.

BASTAWROS, A.-F., BART-SMITH, H. & EVANS, A. G. 2000. Experimental analysis of deformation mechanisms in a closed-cell aluminum alloy foam. *Journal of the Mechanics and Physics of Solids*, **48**, 301–322.

BAUD, P., KLEIN, E. & WONG, T.-F. 2004. Compaction localization in porous sandstones: spatial evolution of damage and acoustic emission activity. *Journal of Structural Geology*, **26**, 603–624.

BÉSUELLE, P. & RUDNICKI, J. W. 2004. Localization: shear bands and compaction bands. *In*: GUÉGUEN, Y. & BOUTÉCA, M. (eds) *Mechanics of Fluid Saturated Rocks*. International Geophysics Series, **89**, 219–321.

BILBY, B. A. & ESHELBY, J. D. 1968. *Dislocations and the Theory of Fracture*, Volume 1. Academic Press, New York, 99–182.

CHALLA, V. & ISSEN, K. A. 2004. Conditions for compaction band formation in porous rock using a two-yield surface model. *Journal of Engineering Mechanics*, **130**, 1089–1097.

COCCO, M. & RICE, J. R. 2002. Pore pressure and poroelasticity effects in Coulomb stress analysis of earthquake interactions. *Journal of Geophysical Research*, **107**, doi:10.1029/2000JB000138.

ESHELBY, J. D. 1957. The determination of the elastic field of an ellipsoidal inclusion and related problems. *Proceedings of the Royal Society of London, Series A*, **241**, 376–396.

FLETCHER, R. C. & POLLARD, D. D. 1981. Anticrack model for pressure solution surfaces. *Geology*, **9**, 419–424.

FÔRTIN, J., STANCHITS, S., DRESEN, G. & GUÉGUEN, Y. 2006. Acoustic emission and velocities associated with the formation of compaction bands in sandstone. *Journal of Geophysical Research*, **111**, B10203, doi:10.1029/2005JB003854.

FOSSEN, H. & HESTHAMMER, J. 1997. Geometric analysis and scaling relations of deformation bands in porous sandstones. *Journal of Structural Geology*, **19**, 1479–1493.

GRUESCHOW, E. & RUDNICKI, J. W. 2005. Elliptic yield cap constitutive modeling for high porosity sandstone. *International Journal of Solids and Structures*, **42**, 4574–4587.

HAIMSON, B. C. 2001. Fracture-like borehole breakouts in high-porosity sandstone: are they caused by compaction bands? *Physics and Chemistry of the Earth (A)*, **26**, 15–20.

HAIMSON, B. C. 2003. Borehole breakouts in Berea sandstone reveal a new fracture mechanism. *Pure and Applied Geophysics*, **160**, 813–831.

HAIMSON, B. & LEE, H. 2004. Borehole breakouts and compaction bands in two high-porosity sandstones. *International Journal of Rock Mechanics & Mining Sciences*, **41**, 287–301.

HAIMSON, B. C. & SONG, I. 1998. Borehole breakouts in Berea sandstone: two porosity-dependent distinct shapes and mechanisms of formation. *In*: *SPE/ISRM Rock Mechanics in Petroleum Engineering*. Society of Petroleum Engineers, Richardson, TX, 229–238.

HILL, R. E. 1989. *Analysis of deformation bands in the Aztec sandstone, Valley of Fire State Park, Nevada.* Master's thesis, University of Nevada, Las Vegas.

HOENIG, A. 1978. The behavior of a flat elliptical crack in an anisotropic elastic body. *International Journal of Solids and Structures*, **14**, 925–934.

HOLCOMB, D. J. & OLSSON, W. A. 2003. Compaction localization and fluid flow. *Journal of Geophysical Research*, **108,** B6,2290, doi:10.1029/2001JB000813.

ISSEN, K. A. & RUDNICKI, J. W. 2000. Conditions for compaction bands in porous rock. *Journal of Geophysical Research*, **105**, 21529–21536.

KATSMAN, R., AHARONOV, E. & SCHER, H. 2006. Localized compaction in rocks: Eshelby's inclusion and the spring network model. *Geophysical Research Letters*, **33,** L10311, doi:10.1029/2005GL025628.

KINNEY, J. H., MARSHALL, G. W., MARSHALL, S. J. & HAUPT, D. L. 2001. Three dimensional imaging of large compressive deformations in elastomeric foams. *Journal of Applied Polymer Science*, **80**, 1746–1755.

KIRBY, S., DURHAM, W. B. & STERN, L. 1992. The ice I–II transformation: mechanisms and kinetics under hydrostatic and nonhydrostatic conditions. *In*: MAENO, N. & HONDOH, T. (eds.) *Physics and Chemistry of Ice*. Hokkaido University Press, Sapporo, 456–462.

KLAETSCH, A. R. & HAIMSON, B. C. 2002. Porosity-dependent fracture-like breakouts in St. Peter sandstone. *In*: HAMMAH, R., BADEN, W., CURRAN, J. & TELESNICKI, N. (eds) *Mining and Tunneling Innovation and Opportunity*, University of Toronto Press, Toronto, 1365–1371.

LAWN, B. 1993. *Fracture of Brittle Solids* 2nd edn, Cambridge Solid State Science Series, Cambridge University Press, Cambridge.

MOLLEMA, P. & ANTONELLINI, M. A. 1987. Compaction bands: a structural analog for anti-mode I cracks in aeolian sandstone. *Tectonophysics*, **267**, 209–228.

MURA, T. 1987. *Micromechanics of Defects in Solids*, 2nd, revised edn. Kluwer, Norwell, MA.

OLSSON, W. A. 1999. Theoretical and experimental investigation of compaction bands. *Journal of Geophysical Research*, **104**, 7219–7228.

OLSSON, W. A. & HOLCOMB, D. J. 2000. Compaction localization in porous rock. *Geophysical Research Letters*, **27**, 3537–3540.

PAPKA, S. D. & KYRIAKIDES, S. 1998. Experiments and full-scale numerical simulations of in-plane crushing of a honeycomb. *Acta Metallurgica*, **46**, 2765–2776.

PARK, C. & NUTT, S. R. 2001. Anisotropy and strain localization in steel foam. *Material Science and Engineering*, **A299**, 68–74.

RICE, J. R. 1968*a*. A path independent integral and the approximate analysis of strain concentration by notches and cracks. *Journal of Applied Mechanics*, 379–386.

RICE, J. R. 1968*b*. Mathematical analysis in the mechanics of fracture. *In*: LIEBOWITZ, H. (ed.) *Fracture: an Advanced Treatise*, Volume 2. Academic Press, New York, 191–311.

RUDNICKI, J. W. 1977. The inception of faulting in a rock mass with a weakened zone. *Journal of Geophysical Research*, **82**, 844–854.

RUDNICKI, J. W. 1980. Fracture mechanics applied to the Earth's crust. *Annual Review of Earth and Planetary Sciences*, **8**, 489–525.

RUDNICKI, J. W. 2002. Alteration of regional stress by reservoirs and other inhomogeneities: stabilizing or destabilizing? *In*: VOUILLE, G & BEREST, P. (eds) Proceedings of the Nineth International Congress on Rock Mechanics, Paris, 25–29 August, 1999, Volume 3. Balkema, Rotterdam, 1629–1637.

RUDNICKI, J. W. 2003. Compaction bands in porous rock. *In*: LABUZ, J. F. & DRESCHER, A. (eds) *Bifurcations and Instabilities in Geomechanics*. Proceedings of the International Workshop on Bifurcation and Instability 2002, St. Johns College 3–5 June, 2002. Swets & Zeitlinger, Lisse, 29–39.

RUDNICKI, J. W. 2004. Shear and compaction band formation on an elliptic yield cap. *Journal of Geophysical Research*, **109**, B03402, doi:10.1029/2003JB002633.

RUDNICKI, J. W. & STERNLOF, K. R. 2005. Energy release model of compaction band propagation. *Geophysical Research Letters*, **32**, L16303, doi:10.1029/2005GL023602.

RUDNICKI, J. W., TEMBE, S. & WONG, T.-F. 2006. Relation between width and length of compaction bands in porous sandstones (abstract). *EOS Transactions*, **87(52)**, *American Geophysical Union, Fall Meeting Supplement*, Abstract T43A-1633.

STERNLOF, K. R. 2006. *Structural geology, propagation mechanics and hydraulic effects of compaction bands in sandstone.* PhD thesis, Stanford University, Stanford.

STERNLOF, K. & POLLARD, D. 2002. Numerical modeling of compactive deformation bands as granular anti-cracks. *EOS Transactions, American Geophysical Union*, **83**, F1347, *Fall Meeting Supplement*, Abstract T11F-10.

STERNLOF, K., POLLARD, D. & CHOPRA, G. 2003. Compaction bands as anticracks in sandstone: taming complexity through integrated observation, experimentation and process based simulation. *Geological Society of America, Abstracts with Programs*, **35**, no. 6, 40.

STERNLOF, K. R., CHAPIN, J. R., POLLARD, D. D. & DURLOFSKY, L. J. 2004. Permeability effects of systematic deformation band arrays in sandstone. *AAPG Bulletin*, **88**, 1315–1329.

STERNLOF, K. R., RUDNICKI, J. W. & POLLARD, D. D. 2005. Anti-crack inclusion model for compaction bands in sandstone. *Journal of Geophysical Research*, **110**, B11403, doi: 10.1029/2005JB003764.

TADA, H., PARIS, P. C. & IRWIN, G. R. 1973. *The Stress Analysis of Cracks Handbook*, Del Research, Hellertown, PA.

TEMBE, S., VAJDOVA, V., WONG, T.-F. & ZHU, W. 2006. Initiation and propagation of strain localization in circumferentially notched samples of two porous sandstones. *Journal of Geophysical Research*, **111**, B02409, doi:10.1029/2005JB003611.

VAJDOVA, V. & WONG, T.-F. 2003. Incremental propagation of discrete compaction bands and microstructural observations on circumferentially notched samples of Bentheim sandstone. *Geophysical Research Letters*, **30**, 1775, doi:10.1029/2003GL017750.

VAJDOVA, V., BAUD, P. & WONG, T.-F. 2004. Permeability evolution during localized deformation in Bentheim sandstone. *Journal of Geophysical Research*, **109**, B10406, doi:10.1029/2003JB002942.

WAWERSIK, W. R., RUDNICKI, J. W., DOVE, P. *ET AL.* 2001. Terrestrial sequestration of CO_2: an assessment of research needs. *Advances in Geophysics*, **43**, 97–177.

WONG, T.-F., BAUD, P. & KLEIN, E. 2001. Localized failure modes in a compactant porous rock. *Geophysical Research Letters*, **28**, 2521–2524.